Using Lunar Observations to Validate In-flight Calibrations of Clouds and Earth Radiant Energy System Instruments

Janet L. Daniels, G. Louis Smith, Kory J. Priestley and Susan Thomas

Abstract— **The validation of in-orbit instrument performance requires stability in both instrument and calibration source. This paper describes a method of validation using lunar observations scanning near full moon by the Clouds and Earth Radiant Energy System (CERES) instruments. Unlike internal calibrations, the Moon offers an external source whose signal variance is predictable and non-degrading. From 2006 to present, in-orbit observations have become standardized and compiled for the Flight Models-1 and -2 aboard the Terra satellite, for Flight Models-3 and -4 aboard the Aqua satellite, and beginning 2012, for Flight Model-5 aboard Suomi-NPP. Instrument performance parameters which can be gleaned are detector gain, pointing accuracy and static detector point response function validation. Lunar observations are used to examine the stability of all three detectors on each of these instruments from 2006 to present. This validation method has yielded results showing trends per CERES data channel of 1.2% per decade or less.**

Index Terms— **Aqua, calibration, CERES, Earth Radiation Budget, Earth Observing System, lunar measurements, Moon, radiometry, remote sensing, satellites, telescope, Terra, validation**

I. INTRODUCTION

CLOUDS and Earth Radiant Energy System (CERES) instruments have three radiometers each: a total channel which measures radiation from the Earth, both emitted and reflected solar, a shortwave channel for reflected solar radiation, and a channel for measuring radiation from the Earth through the longwave atmospheric window. Flight Models (FM) -1 and FM-2 are currently flying on the Earth Observation System (EOS) AM-1 satellite, Terra; FM-3 and FM-4 are orbiting onboard the EOS PM-1 satellite, Aqua; and FM-5 is operating on Suomi-NPP. The objective of the CERES project is to make measurements from which the radiation fluxes over the Earth can be computed to an accuracy of 1% for shortwave fluxes and of 0.5% for outgoing longwave fluxes [1]. To achieve the needed level of accuracy requires that CERES instruments be calibrated frequently in orbit, and these results must be validated by comparisons among the instruments to assure continuity of the Radiation Budget Climate Data Record (RBCDR) [2]. With the CERES instruments aboard three separate spacecraft in distinctly different orbits,

comparisons among the instruments provide confidence for the accuracy of the RBCDR [3].

CERES FM-6 is scheduled to fly aboard the JPSS-1satellite in 2018 and a successor to CERES is planned for the JPSS-3 satellite, to be launched in 2023. Since the design goal of CERES is five years, FM-5 may be the sole operational instrument by the time FM-6 is launched. Accuracy requirements demand an overlap period between succeeding instruments to maintain the continuity of the RBCDR. A premature failure of an instrument could jeopardize this continuity. Although many Earth scenes have been suggested, there are always concerns for the adequacy of the results. This paper addresses the use of the Moon as a calibration target for CERES instruments.

The Moon is a useful, independent calibration target and provides an extremely stable surface [4]. The Sea-viewing Wide Field-of-view Sensor (SeaWiFS) and Moderate Resolution Imaging Spectro-radiometer (MODIS), have used the Moon as a calibration target successfully. These instruments all have high spatial resolution such that the instrument field of view is filled by the Moon's image, and a particular site on the Moon may be selected as target [5]-[6]. Unlike imagining instruments that view a small subset of the lunar surface, CERES detectors register the signal output reflected off of the entire face of the Moon, but lunar irradiance is small compared to the dynamic ranges of the CERES channels. The size of the Moon's image within the FOV varies with respect to lunar distance from the Earth. Solar irradiance on the Moon varies with respect to solar distance. Lunar librations and phase angles result in viewing the Moon from different directions and with different solar illumination over the observed surface. These effects create a variation in lunar irradiance of 20% in the total channel and 8% in the shortwave channel. However, these variations are systematic. This paper demonstrates that lunar observations can be used to validate CERES radiances to the required accuracy.

II. CERES LUNAR OBSERVATION METHOD

Due to the differences in their orbits, Terra and Aqua spacecrafts observe the Moon over opposite poles of the Earth. FMs-1 and -2 on Terra perform lunar observations while over the North Pole, and FMs-3 and -4 on Aqua observe the Moon over the South Pole, shown in Fig. 1.
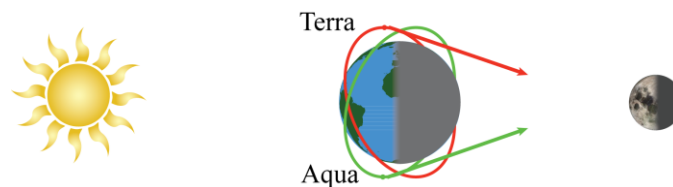

Fig. 1. Terra and Aqua orbital locations during lunar observations. The geolocated positions of these satellites are at polar-opposite angles.

A rotation of the CERES instrument in azimuth will bring the Moon into view between the nadir side of each instrument and the limb of the Earth. Given the ephemeris of the Moon and of each satellite, the location of the Moon in CERES instrument coordinate, i.e. azimuth and elevation angles, can be computed so that lunar observations can be made. As each satellite moves along its orbit, the Moon sets below the limb of the Earth. The CERES instrument is rotated in azimuth and the elevation angle is set so that the Moon moves through the CERES FOV. With the elevation angle fixed, the instrument scans in azimuth over a 12.9° range at a rate of 4°/s until the Moon has passed from the plane of the FOV, then the elevation angle is reset to a lower position and the process is repeated. Instrument azimuth angles are defined for each orbit to limit FOV scanning between two positions where full lunar coverage with a spacelook per scan is taken. These azimuth values are calculated for up to three different elevation positions per orbit to ensure maximum data coverage per phase angle. CERES slews to the first elevation position ahead of the moon, and azimuth scanning begins. The moon drifts through instrument elevation plane. An average of 10 scans in azimuth are taken for each elevation position. If more than one elevation position is to be used, the instrument slews to the next elevation plane and azimuth scanning continues. An illustration based on actual track data is shown in Fig. 2. Satellite ephemeris and instrument position information is used to adjust lunar position across the FOV. The standard elevation positions for lunar observations are -7.78°, -12.78° and -17.78°. Due to instrument interference with the -7.78° position and signal interference with the high-gain antenna on Suomi-NPP at the -12.78° position, updated scanning positions were updated to -13.78°. -17.78° and -21.78°.
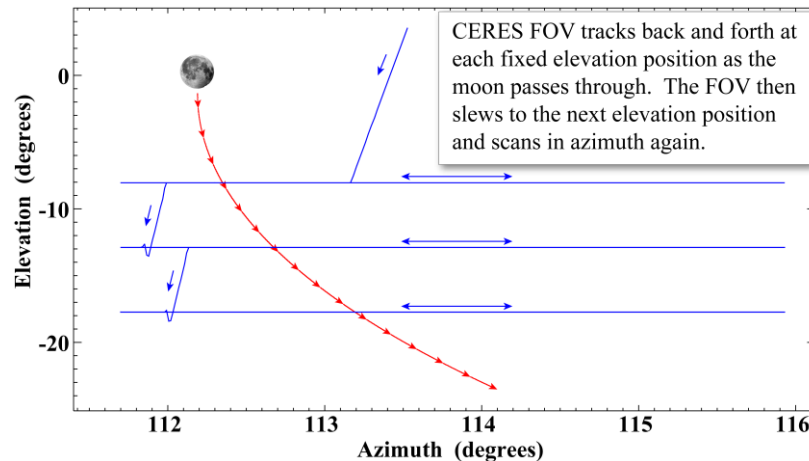

Fig. 2. Apparent movement of Moon with respect to the CERES axis.

CERES detectors were not designed to withstand direct sunlight. As a preventative measure against causing inadvertent detector damage due to direct incoming solar radiation, no instrument commanding is performed during times when the Sun's elevation position is between -30° to 5° with respect to the CERES X-Y axis. Although during lunar observations, the detectors

are pointed away from the solar presence, no exception to this standard operating procedure is performed thereby preventing any threat to instrument health and safety. At times, commanding is delayed until this danger zone time period is completed. Therefore, due to orbital variability throughout the year, lunar observation orbits will include scans from one to three elevation positions.
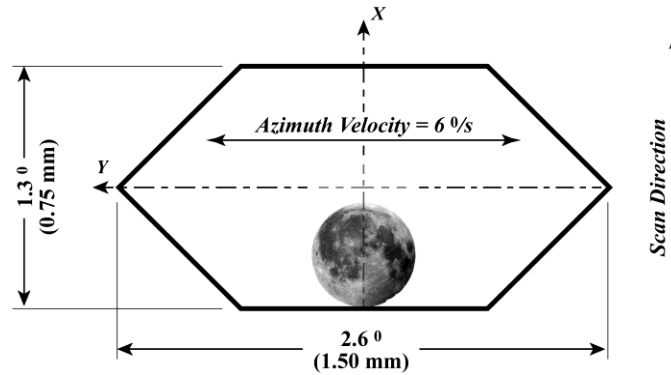
Fig. 3. Moon in CERES field of view

Fig. 3 shows the moon within the field of view of CERES. The FOV is a hexagon 2.6° across the corners and 1.3° between the sides. From mean Earth-Moon distance, the Moon is a circle with diameter 0.52°. Due to spherical aberrations of the telescope mirrors, there is a blur circle at the aperture that defines the FOV, so that the image must be within the FOV by 0.16° to measure the full lunar irradiance.

As designed, the detector should have a uniform response to radiation over its surface, so that the static point response function is determined by the field stop. Azimuth scan-rate during lunar observations is faster than Moonset rate by an order of magnitude. These in-orbit observations are taken at a lower azimuth scanning rate when compared to ground testing. Therefore, data points are much closer than for standard pre-launch ground calibrations, and the detector can be mapped with greater precision.

The angle between the subsolar point and the subearth point on the Moon is denoted as the phase angle and is the dominant factor in lunar irradiance. Since these observations are limited to a narrow time window per orbit, observing the moon at specific phase angles is not possible. Therefore, CERES lunar observations are timed to occur over a specific lunar phase angle range of approximately [-10° to -5°], fullest moon, and [5° to 10°]. Although the individual observations per orbit are completed within minutes, the series of observations occur over a period of 18 hours centered at full moon.

III. EXTRACTING AND STANDARDIZING THE DATA

Lunar observations from all three channels of the CERES instruments are used in this study. The total channel consists of a Cassegrain telescope which collects radiation, nominally between 0.2 μ and 100 μ onto a detector. The response of the channel to incoming radiation is not constant for all wavelengths but varies due to the spectral reflectivity of the two mirrors and the spectral absorptivity of the detector.   Fig. 4 shows the nominal spectral response of the CERES detectors. The shortwave channel is the same as the total, but has two quartz filters which limit the radiation from 0.2 μ to 5.0 μ. Likewise, the window channel has filters to restrict the spectral response to 8 μ to 12 μ. The instrument thus measures "filtered" radiances. To get meaningful radiances from the Earth, it is necessary to account for the spectral responses of the channels, producing "unfiltered" radiances. This investigation does not attempt to account for the spectral responses of the instruments to measure the Moon's irradiance, but examines the filtered radiances so as to validate the stability of the measurements. To obtain the highest quality in the dataset and to avoid issues with optical blurring when scanning on and off the moon, the detector output is interpolated for each detector in an area bracketing the lunar position which includes data where the FOV is completely off of the moon in all directions.
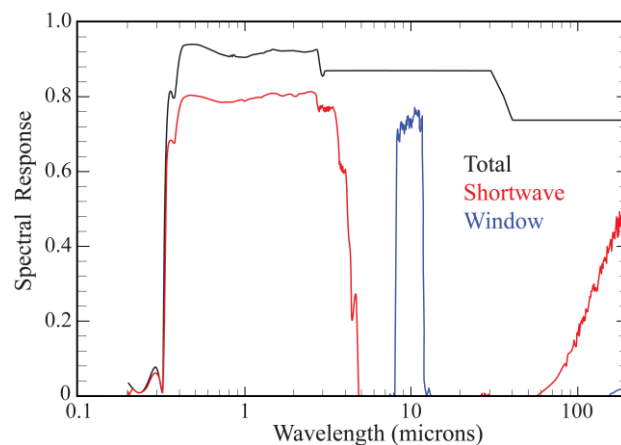

Fig. 4. Spectral Responses of the CERES detector channels

During in-orbit operations, the response of the instrument to radiation changes, in part due to changes of the spectral responses of each channel. Data from the first six months of operation are processed using ground calibrations. Internal calibration devices are used to calibrate the instruments about every six months thereafter. These data products are Edition 1 C-V (calibration and validation) and are used in this study.

The responses of the CERES detectors are not ideally uniform, but vary with location over each detector surface. This response has been mapped by use of lunar observations [7]-[8]. The goal for using multiple elevation positions during lunar observations is to obtain as much mapping data as possible to provide the highest quality coverage for each detector.

The data from each orbit are mapped in FOV elevation and azimuth and provide a detailed mapping of each detector. Due to slight variations in lunar declination, some observation orbits contain more precisely spaced detector coverage than others due to the number of elevation positions available per phase angle and spatial distribution of data points across the detector.
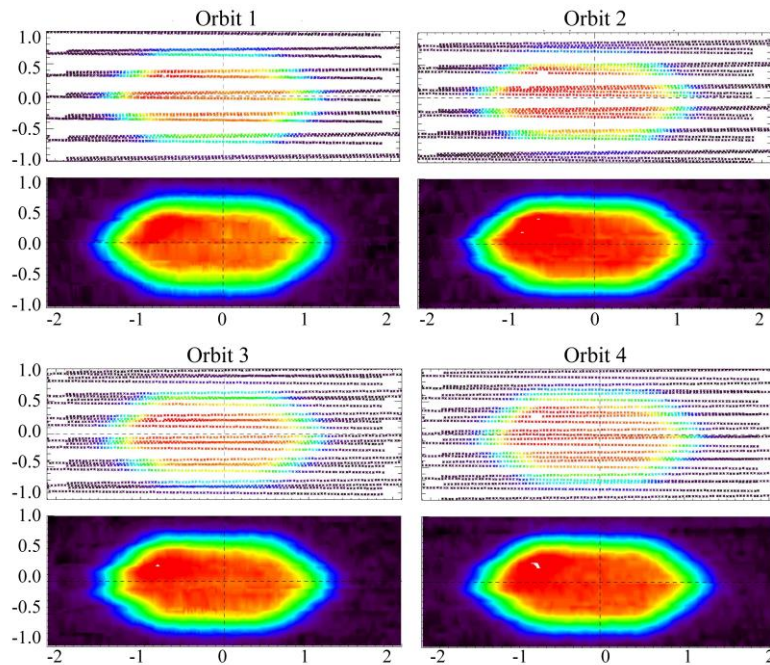

Fig. 5. Samples of variations in detector coverage due to different lunar elevation sink rates. The upper plots show individual measurements. The lower plots show interpolated measurements.

Although every lunar observation since 2006 has been programmed using the same formulas for timing and position, the data coverage of the FOV for each orbit varies greatly due to lunar elevation sink rate. To differentiate between orbits containing good detector coverage, a quality number is calculated and assigned to each mapped detector data set. This number is derived by selecting FOV elevation data points near FOV azimuth=0.0. These data points are sorted, differenced, and the standard deviation of the difference is calculated. The lower value, the more evenly distributed the data are across the detector. The examples shown above in Fig. 5 are taken in consecutive orbits, each containing scan data from 2 different instrument elevation positions. The quality values range left-to-right from 0.0923 to 0.0336.
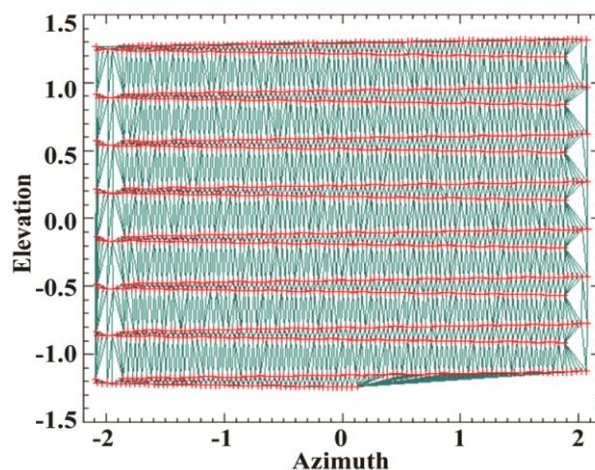
Fig. 6. Distribution of data across the FOV (red), with Delauney triangulation of the initial irregular data grid (green).

No two lunar observations contain the same azimuth and elevation positions. Therefore to improve detector analysis, valid data from each orbit must be translated into a standard angular grid for improved long-term trending and comparison. Fig. 6 shows a sample of data taken from one orbit of lunar observation showing the track of the moon across the CERES detector as the instrument scans in azimuth and the moon sets across the elevation plane of the FOV (actual data points are shown in red). The irregularly-gridded data is used to create a Delauney triangulation of planar set points, shown in green. Values are calculated at each triangle vertex to interpolate values along a regular grid. For Lunar observation data, the standard grid used ranges from [-2º,2º] in azimuth and [-1º,1º] in elevation with a spacing between points of 0.01º in both directions. The surface plot in Fig. 7 shows the resulting gridded data set.
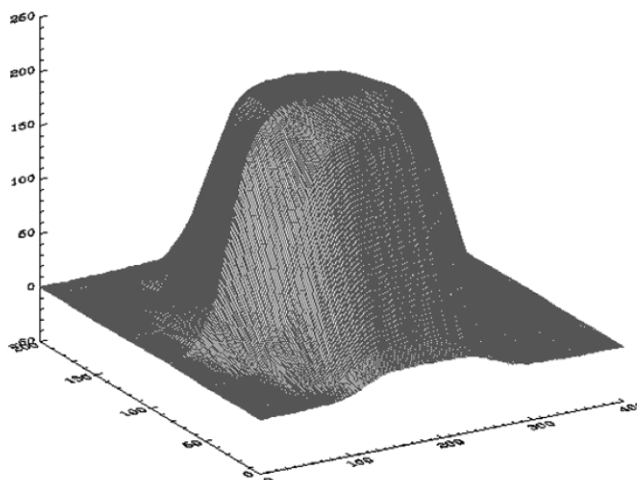

Fig. 7. Interpolated spatially-gridded data

Additional validation of the translation from non-gridded to gridded data includes both data sets in a 3D plot. One orbit of valid data is plotted at a time using the original azimuth and elevation data where each channel detector output is byte-scaled and

color-coded, a sample of which is below in Fig. 8. Resulting gridded data is shown as the contoured transparent data using the same byte-scaled color translation. Once data have been translated into a standardized grid, orbital geometry effects are addressed.
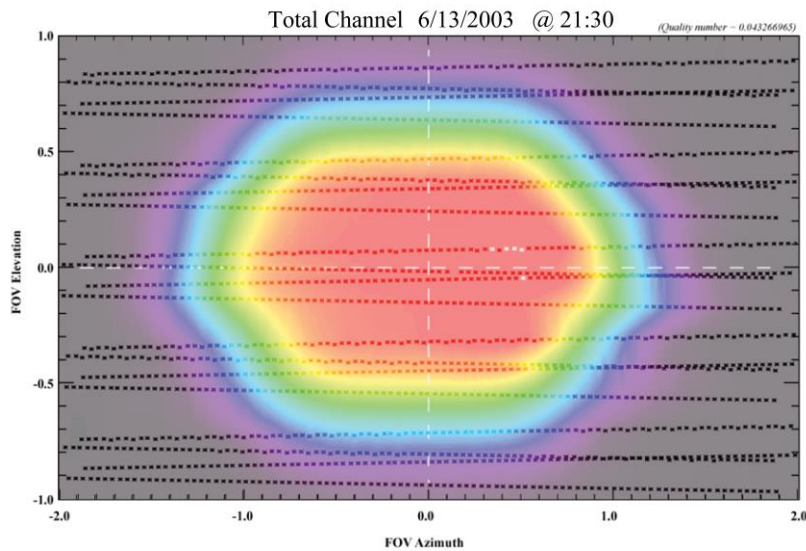

Fig. 8. Irregular vs. standard grid translation comparison

IV. ADJUSTING FOR ORBITAL EFFECTS

The spectral radiance $L_\lambda(\alpha, \beta)$ varies over the surface of the Moon due to variations in distance from Earth-to-Moon and Sun-to-Moon, solar phase angle over the lunar surface, spectral albedo over the surface, and bidirectional reflectance of the surface. If the Moon were always oriented so that the instrument always saw the same view of the Moon, the spectral irradiance would vary only due to the distance to the Sun and the distance to the instrument. With these distances taken into account, the measurement would then vary due to changes of the gain of the channel or of the spectral response. However, as the Moon moves around its elliptical orbit with a constant rate of rotation, the sub-Earth point (i.e. the point at which the line from center of the Earth to the center of the Moon intersects the lunar surface) moves. This change of orientation of the Moon as seen from Earth is called libration. Likewise, the sub-solar point on the Moon varies. The results of these variations are about 1% of the irradiance. Because of the variation in spectral albedo of the lunar surface, the librations will change the spectral irradiance at the instrument.

Assuming the point response function to be uniform over the FOV, the measured irradiance of the j-th channel will be the integral over the Moon's disc S of the spectral radiance $L_\lambda(\alpha, \beta)$ at location defined by the selenodetic latitude and longitude α, β, integrated over wavelength weighted by the spectral response function $S_j(\lambda)$ of the channel

$$m_j = \int_0^\infty d\lambda S_j(\lambda) \int_S \, d\,\Omega L_\lambda(\alpha, \beta) \qquad (1)$$

The inner integral is the spectral irradiance at the instrument. The $d\Omega$ is a differential area element of the lunar image and the range of the inner integral S is the area of the image. The diameter of the image varies inversely as the distance from Earth to Moon, so S varies inversely as the square of the Earth-Moon distance. The spectral radiance consists of emitted (longwave) radiation and reflected solar (shortwave) radiation.
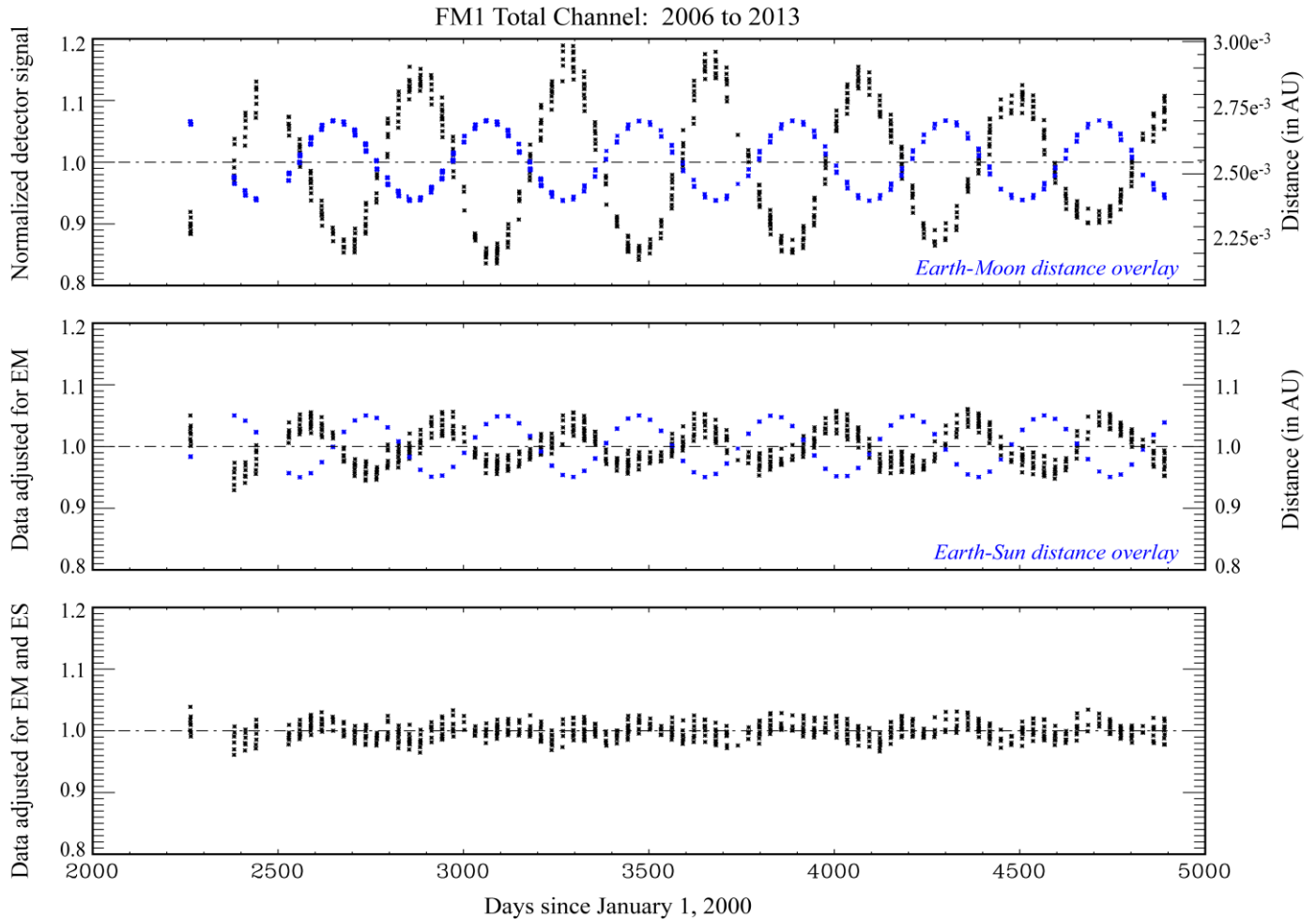

Fig. 9. a) Variation of Total channel output (black, interpolated and normalized) and Earth-Moon (EM) distance curve-shape overlayed (blue) with time, b) Variation of Earth-Moon-adjusted FM-1 Total channel output (black) and Earth-Sun (ES) distance curve-shape overlayed (blue), c) FM-1 Total channel output after Earth-to Moon and Earth-to-Sun adjustment.

For each lunar observation orbit, data from the standardized grid of [-2º,2º] in azimuth and [-1º,1º] in elevation is interpolated into a single value for overall radiance for each detector. Day 1 corresponds to 1 January 2000. The resulting data is normalized using the mean of the entire dataset and is shown in Fig. 9a for FM-1 Total Channel (black data points).

Output is cyclic and is found to be dependent on the following in order of magnitude: Earth-Moon (EM) distance, Earth-Sun (ES) distance, lunar phase angle and lunar libration. Values for EM are normalized by the mean EM distance, and ES is expressed in AU. This order of importance becomes clear when comparing the cyclic nature of each of the above factors.

In Fig. 9a, note the increasing and diminishing detector output as EM and ES phase into and out of each other. Observe the magnitude of the signal around day 3300 and compare it with the magnitude of day 4500. At day 3300, both the sun and the

moon are synchronized at apogee and perigee, causing greater fluctuation in the detector channel output. Detector fluctuation decreases near day 4500 as the solar and lunar orbits become out of phase. Both EM and ES effects are removed from the data using the inverse square. Fig. 9b includes both the Total detector data when adjusted for EM (black) and ES curve shape with its correlation. Cyclic variations are dramatically reduced, and the resulting data are plotted in Fig. 9c.
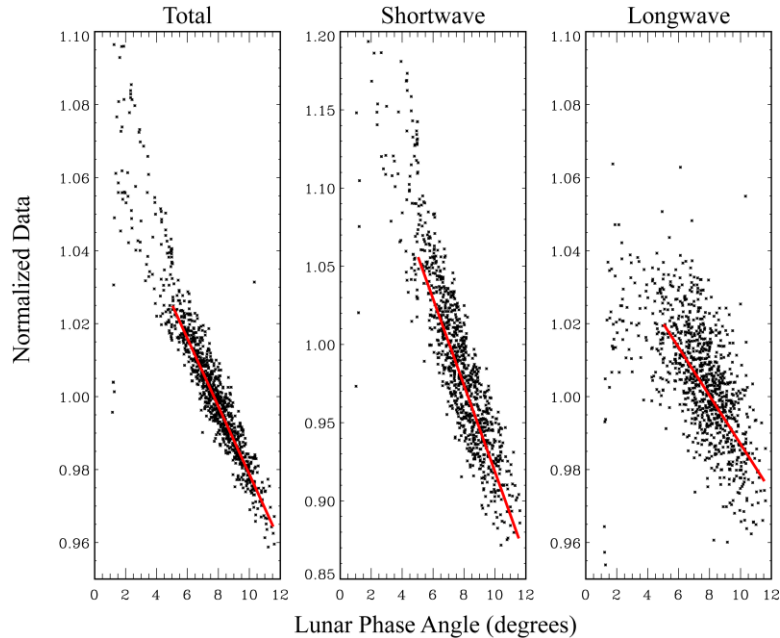

Fig. 10. Lunar Phase Angle and CERES detector response

   Once the effects of orbital distances are removed, the next data adjustment to be applied concerns lunar phase angle. The measurements for all three FM-1 detectors channel with the effects of Sun-Earth and Earth-Moon distances removed are shown as a function of phase angle in Fig. 10. The flare of lunar irradiance is apparent as the phase angle approaches 0°. For phase angles smaller than 5°, the lunar reflectivity increases significantly [9]. For this study, data are constrained to phase angles of 5° and greater where the relation between detector response and phase angle is linear and inversely proportional. The plots in Fig. 10 cover almost 7 years of lunar calibration data per orbit. Thus far, no averaging or smoothing of the data has been performed. Lunar phase angle gradually decreases as full moon approaches and increases afterward. As expected, shortwave channel is most affected with changes in the amount of reflected sunlight. Total channel exhibits a high degree of consistency, and even longwave with its much smaller sensitivity range shows some dependency. Over the short time period for each monthly set of calibrations, the removal of phase angle effects results in decreasing the variation in detector signal for each month. Fig. 11 shows each of the three FM-1 detectors after which EM and ES have been adjusted but before phase angle effects have been removed.
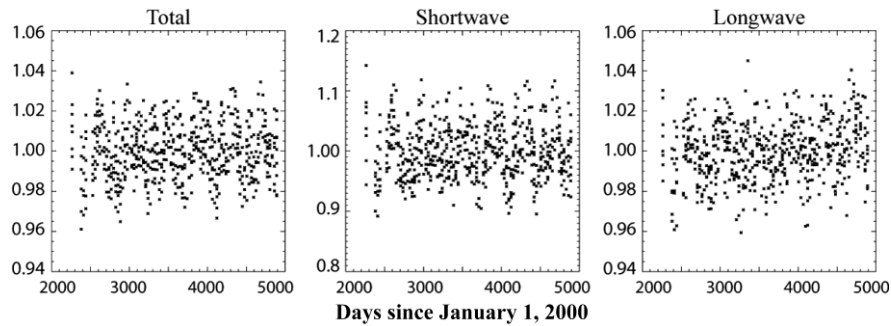
Fig. 11. CERES FM-1 detector response before lunar phase angle adjustment.

Fig. 12 shows the responses of the three channels of FM-1 after EM and ES distances are taken into account and the effects of

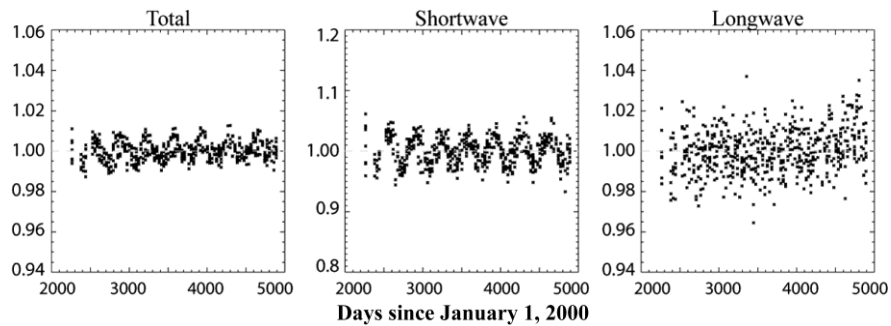phase angle are removed by the lunar relations shown by Fig. 10.

Fig. 12. CERES FM-1 detector response after lunar phase angle adjustment.

   With this decreased monthly variability, another cyclic pattern becomes clear in total and shortwave channel data. The total

channel has a nearly cyclic variation of +/-0.01 and the shortwave channel shows a variation of +/-0.05. The window channel has

a random scatter of +/-0.02. Slight variations in reflectivity were found to be due to librations in lunar latitude. Up to this point,

the CERES instruments for Terra and Aqua exhibit the same effects for orbital adjustments. Now, CERES data becomes more

location specific where the slight differences in orbital viewing angle of the Moon for each satellite shows polar positional

dependences. To understand why this would occur, consider the surface reflectivity of the Moon as seen in Fig. 13.

Fig. 13. Image of the Moon

The majority of the darker mares are located in the northern lunar hemisphere. However, a brighter band of terrae appear at the northern most place when the moon librates in such a way that the northern pole rotates slightly toward Earth. When the suborbital position of Earth in latitude drifts into the northern lunar hemisphere, the view from Earth includes more of these dark mares. Likewise, when the suborbital latitude of Earth drifts into the southern hemisphere, the view from Earth includes more of the bright terrae. The CERES total and shortwave detectors are sensitive enough to make satellite-to-moon viewing angles important. Dependencies based on libration latitude were found to be highly satellite specific. Terra and Aqua instruments also observed the moon at physically opposite angles. If the orientation of Terra's FMs-1 and -2 at Earth's North Pole is given as "right-side-up", then the orientation of Aqua's FM-3and -4 at the South Pole views the moon "upside-down". This causes the libration versus detector output plots to be reversed from each other for Aqua and Terra. For Terra's FMs-1 and -2, the increase in reflectivity at the moon's northern pole is not evident. Total and shortwave detectors exhibit an almost linear relation to libration latitude as shown in Fig. 14a. Any given point on the surface of the Moon will be close to thermal equilibrium, so that the total radiation flux from the point will equal the incident solar flux. If the Moon were a Lambertian reflector and emitter, the total radiance from the point toward the instrument would not vary with albedo. The changes of the total channel response with librations are due to anisotropy of reflected and emitted radiation. The total channel thus changes much less with albedo variations than the shortwave channel does.

In Figs. 14 and 15, detector data per orbit is shown in black and a 2nd order fit to the data is in red. This relation is used to adjust the data for these effects of libration.
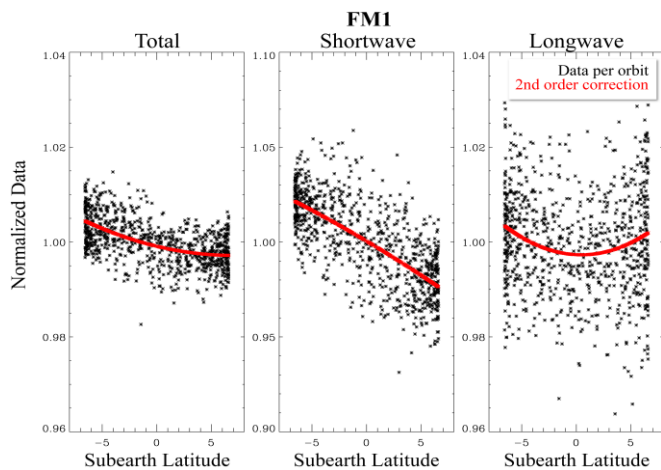

Fig. 14. FM-1 detector output versus lunar libration latitude.   Fig. 15. FM-3 detector output versus lunar libration latitude
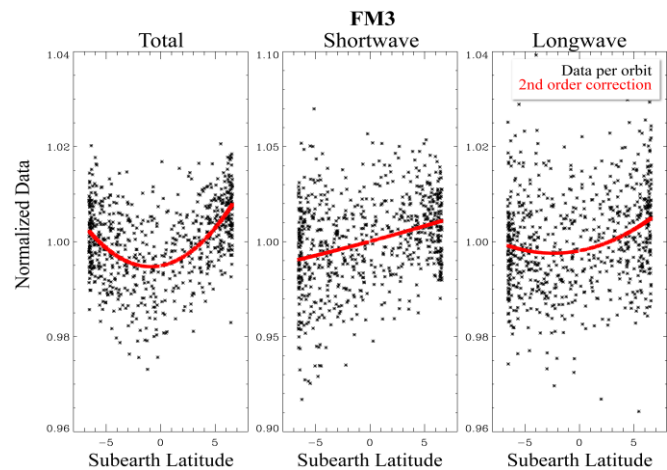
The next series of plots show results when adjusting for lunar libration latitude. No data averaging was performed to obtain the final results shown as black data points. The monthly averaged data in blue are included to aid in verifying that no additional repeatable effects remain. Final actual data are plotted as a percent change in detector output for each channel. Trends for FM-1

(Terra) are shown in Fig. 16, and for FM-3 (Aqua) are shown in Fig. 17. Table 1 summarizes the decadal trends per instrument

channel for each instrument.

Table 1. Resulting trends in detector stability as extracted from lunar observations

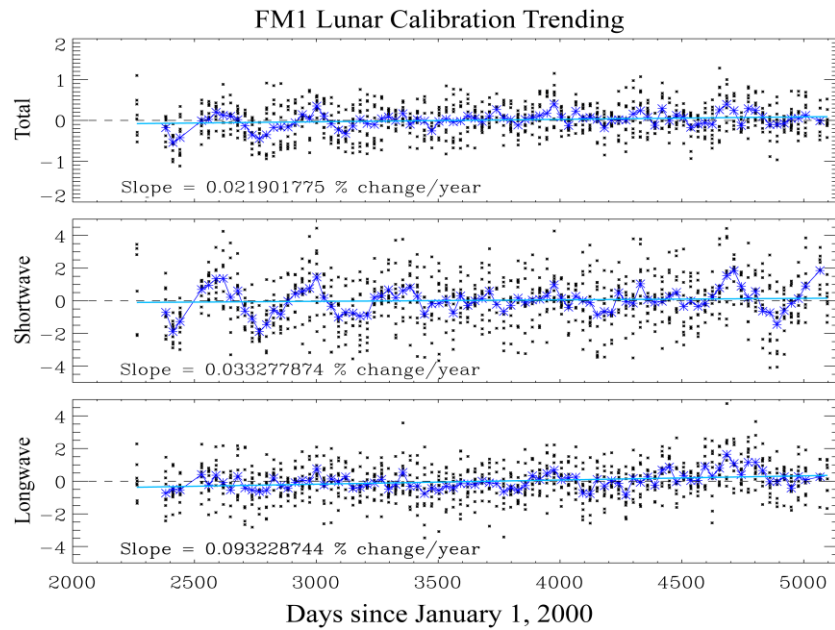| FM	Total Channel	Shortwave Channel	Longwave Channel
FM-1	0.2190 % / decade	0.3328 % / decade	0.9323 % / decade
FM-2	0.2931 % / decade	-0.3926 % / decade	0.4221 % / decade
FM-3	1.1861 % / decade	1.1610 % / decade	0.1851 % / decade
FM-4	0.4890 % / decade		0.2370 % / decade

Fig. 16. Resulting trends in FM-1 detector stability extracted from lunar observations

FM3 Lunar Calibration Trending

Slope = 0.11861283 % change/year

Slope = 0.11605769 % change/year

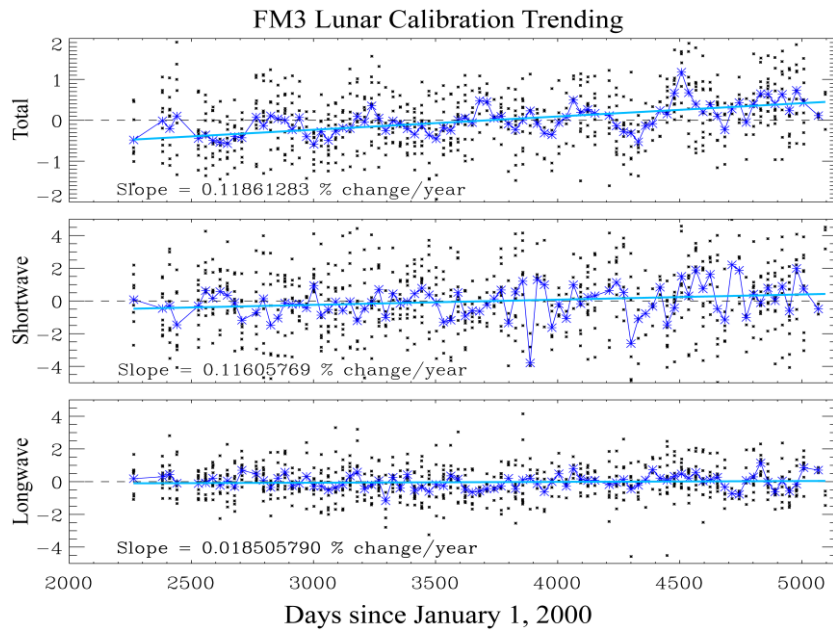Slope = 0.018505790 % change/year

Days since January 1, 2000

Fig. 17. Resulting trends in FM-1 detector stability extracted from lunar observations

Fig. 18 shows the annual running average for each CERES instrument detector. Scale range for the Y-axis has been set to the permitted error ranges allowed in the Radiation Budget Climate Data Record (RBCDR) which are 0.5% for Outgoing Longwave Radiation (OLR) in the total channel detectors and 1.0% for reflected solar in the shortwave channel detectors. CERES longwave channels sample a very narrow slice of emitted heat energy and, thus, have no set error criteria as defined in the RBCDR.

Annual Running Average 2006-2013

FM1 FM3
FM2 FM4

Scale range = RBCDR error permitted (0.5% for OLR)

Scale range = RBCDR error permitted (1.0% for reflected)
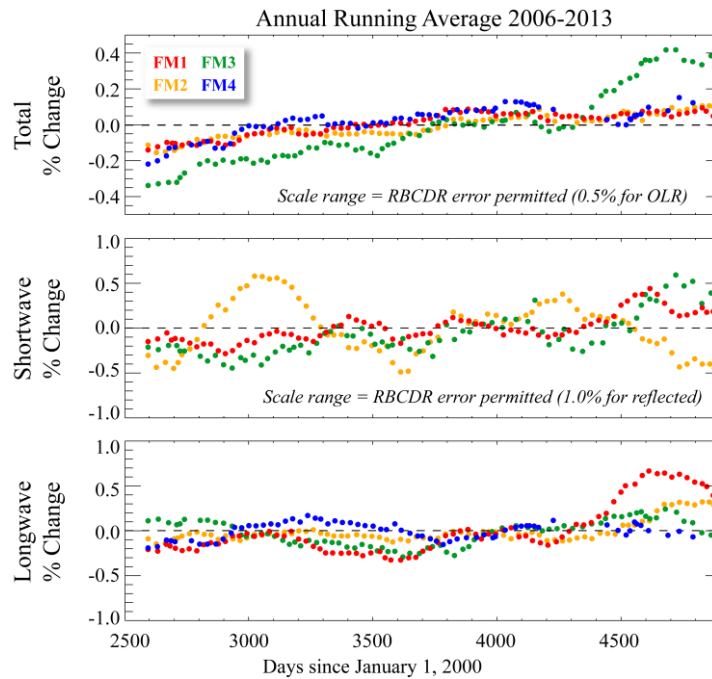
Days since January 1, 2000

Fig. 18. Comparison between CERES detector trending of lunar observations with RBSDR permitted error.

V. DISCUSSION

The procedure demonstrated here provides an independent validation of the in-flight calibrations of the CERES Flight Models -1 through -4. The calibrations of these instruments are not independent, as comparisons have been made since Aqua was placed in orbit. Consequently these instruments must be considered as a set, with the Internal Calibration System of each instrument supported by the other three. The lunar observations validate the efficacy of the ICS to 1% per decade. Moreover, it is possible to use the lunar results to remove these variations. Having established the lunar irradiance and its variations, the major uncertainties of the instruments are the changes of the spectral responses of the channels due to possible in-orbit contamination and degradation.

Although variations in irradiance at first appear to render lunar observations too chaotic as a dependable resource for CERES calibration, knowledge of lunar orbital data reveals systematic, mathematical methods to remove most of these variations. The CERES instruments are found to measure lunar irradiance with consistent high precision which is revealed as each orbital effect is removed. By using a stable, predictable, independent source, calibration source instability can be removed from the equation. Without an independent and stable source, it is unknown if the on-board calibration devices have changed over time. This study provides a capability to identify and adjust for these changes, thereby assisting in the validation of CERES instrument detector stability and improving the quality of the CERES data used to detect climate change.

The librations of the Moon do not exactly repeat from year to year; nevertheless the differences of the irradiances are quite small so that a one-year average of monthly lunar observations has very small variations. When comparing the mean irradiance with that of another instrument, there may be a bias due to differences of the spectral responses. For CERES instruments the spectral responses are similar for a given type channel of all models so that comparisons give very close results for all models.

This paper has used only the filtered radiances. To retrieve the unfiltered irradiances, characterization of the spectra of lunar emitted radiation and of solar radiation reflected by the Moon would be required.

In the future, it is likely that only one Radiation Budget Instrument will be operational at any one time. Planning should provide for an overlap period between instruments to make the RBCDR seamless. In the contingency that a single instrument may fail before being replaced, lunar observations give the possibility of relating the replacement RBI data record to the preceding record. The accuracy with which two instruments can be compared using lunar observations depends on how well the spectral responses are characterized, as well as the lunar spectral reflectivity and emissivity. An error analysis would be needed for each specific instrument.

VI. Conclusion

It is demonstrated that validation of the consistency of calibration of all CERES instruments over time is possible using lunar observations. These standardized observations have been made near full Moon by CERES instruments since 2006. The Moon's surface is very stable, but the illumination and viewing conditions are quite variable, so that measurements of lunar irradiance by CERES have 20% variations. When Earth-Moon distance is taken into account, the variations are reduced to 5%. Removal of Sun-Moon distance effects leaves a variation of 2%. This variation is largely because of the flare of lunar irradiance for phase angles less than 10°. For phase angles between 5° and 10°, the flare is linear and the data can be adjusted to remove this effect, so that quasi-cyclic variations with 1% amplitude remain due to lunar librations. These variations were found to be dependent on the latitude of the lunar subsatellite point. Once this remaining effect is adjusted, the linear trends fitted to these residual changes have slopes of 1.2% per decade or less. A long-term data set spanning several years was required to obtain the necessary range of seasonal orbital effects to demonstrate the robustness of the results. This procedure provides validation of the CERES radiances. The results demonstrate the stability of the CERES Internal Calibration System design.

References

[1] Priestley, Kory J., et. al., Radiometric Performance of the CERES Earth Radiation Budget Climate Record Sensors on the EOS Aqua and Terra Spacecraft through April 2007. *J.Atmos. Oceanic Technol.*, *28*, 3–21, 2011.

[2] Smith, G. L. Peterson, R. B. Lee III, and B. R. Barkstrom, Optical design of the CERES telescope. Earth Observing Systems VI, W. L. Barnes, Ed., International Society for Optical Engineering (*SPIE Proceedings, Vol. 4482*), 269, doi:10.1117/12.453463, 2001.

[3] Priestley, K. J., N. G. Loeb, S. Thomas and G. L. Smith, CERES FM5 and FM6: continuity of observations to support a multi-decadal earth radiation budget climate data record, *Proc. SPIE 7807*, Earth Observing Systems XV, 78070N, Sept. 23, 2010.

[4] Kieffer, H. H., T. C. Stone, The Spectral Irradiance of the Moon. *The Astronomical Journal* (129: 2887-2901), June 2005

[5] Thomas C. Stone, Radiometric Calibration Stability and Inter-calibration of Solar-band Instruments in Orbit Using the Moon. *Proc. SPIE 7081* 70810X-1-8, 2008.

[6] Xiong, X., Z. Wang, J. Sun, A. Angal, J. Fulbright, and J. Butler, MODIS and VIIRS lunar observations and applications. *Proc. SPIE 8889, Sensors, Systems, and Next-Generation Satellites XVII*, 88890V , 2013.

[7] Priestley, K. J., S. Thomas, and G. L. Smith, Validation of Point Spread Functions of CERES Radiometers by the Use of Lunar Observations. *Jour. Atmos. & Ocean. Tech.*, *27*, 1005-1011, 2010.

[8] Daniels, J.L., S. Thomas, G.L. Smith and K.J. Priestley, The point response functions of CERES instruments aboard the Terra and Aqua spacecrafts over the mission-to-date. Imaging Spectrometry XVII, (*SPIE Proceedings, Vol. 8515*), doi:10.1117/12.928499, Oct. 2012

[9]   Pohn, Radin and Wildey, 1969, The Moon's Photometric Function Near Zero Phase Angle from Apollo 8 Photography. *The Astrophysical Journal, Vol.*

        157, Sept 1969.

Janet L. Daniels received her BS degree in mathematics with departmental honors from Christopher Newport University in 1991.

She began working at Langley Research Centre in 1990 as a summer intern. After graduating from college, she became a Mission Operations Specialist with HALOE from 1991 until 2005 when the satellite was decommissioned. Her responsibilities were instrument command and control, health and safety, and analysis of instrument and orbital effects in the science data. She was the sole person responsible for day-to-day operations for the last seven years of the instrument. She has been with the CERES team since 2005, first as a Mission Operations Specialist and now as Senior Science Analyst at NASA Langley. She has published conference papers with SPIE Imaging Spectroscopy.

Ms. Daniels has received many company awards for Outstanding Achievement and several NASA Group Achievement Awards for HALOE and CERES.

G. Louis Smith received his BS degree in aeronautical engineering from Virginia Polytechnic Institute in 1960 and his M.S. and Ph.D. degrees in aerospace engineering in 1963 and 1968.

He began working at Langley Research Centre as a Co-op Student in 1956 and retired in1997 as a Senior Researcher. He has worked since then as a contractor, presently with SSAI at Langley. He has published numerous journal articles and many conference papers.

Dr. Smith has received Langley's H.J.E. Reid Award for Outstanding Technical Paper published at LaRC, the NASA Medal for Exceptional Scientific Achievement, and a Group Achievement Award for the Earth Radiation Budget Study, which led to the Earth Radiation Budget Experiment project.

Kory J. Priestley received his BS degree in mechanical engineering from California Polytechnic State University-San Luis Obispo in 1992, then his MS degree in mechanical engineering in 1993 and Ph.D. degree in 1997 from Virginia Polytechnic Institute and State University.

He began work at Langley Research Centre in 1995 as a graduate co-op student and as an aero-space technologist in the Atmospheric Sciences Division in 1997. He has worked on the CERES project and is the Instrument Scientist for CERES. He has the responsibility for the ground calibration, in-orbit operation and calibration of the CERES instruments, including the FM-5, which was recently launched. His work includes the generation of instrument products to be further processed into scientific data products. He has published numerous journal articles and conference papers. Dr. Priestley was awarded the NASA Medal for Exceptional Achievement.

Susan Thomas is a Lead Scientist in the CERES Instrument group at NASA Langley Research Center, employed with Science Systems and Applications Inc (SSAI) in Hampton, Virginia. She received her BS degree in Physics from University of Kerala, India, MS degree in Physics from University of Cochin, India and her MS degree in Computer Science from Old Dominion University, Norfolk Virginia. She has been involved in the CERES instrument operations, ground test and on-orbit calibration of the instruments, conversion algorithms and validation protocol for the sensor measurements. She has published several journal and conference papers, and has received NASA Group Achievement awards for her work on CERES instruments.